# Voltage Modulation Using Virtual Positive Impedance Concept for Active Damping of Small DC-Link Drive System

Wang, Dong; Lu, Kaiyuan; Rasmussen, Peter Omand; Mathe, Laszlo; Feng, Yang; Blaabjerg, Frede

*Published in:*
IEEE Transactions on Power Electronics

*DOI (link to publication from Publisher):*
10.1109/TPEL.2018.2799988

*Publication date:*
2018

*Document Version*
Accepted author manuscript, peer reviewed version

# Voltage Modulation Using Virtual Positive Impedance Concept for Active Damping of Small DC-Link Drive System

Dong Wang, *Member*, *IEEE*, Kaiyuan Lu, *Member*, *IEEE*, Peter Omand Rasmussen, *Member*, *IEEE*
Laszlo Mathe, *Member*, *IEEE*, Yang Feng, and Frede Blaabjerg, *Fellow*, *IEEE*

***Abstract*—Small DC-link drive systems, built with film capacitor in the DC link, present a new trend in many industrial applications and is obtaining increasing interests. It has the advantages of longer lifetime and the possibility to achieve a more compact design of the capacitor bank, especially at medium and high power rates. However, it could exhibit instability problems, mainly in the form of oscillations. The unexpected oscillation may result in overvoltage and shorten the lifetime of the power devices and the dc-link capacitors; increase the total harmonic distortion (THD) and also the partially weighted harmonic distortion (PWHD) of the grid supply current. Therefore, active damping methods are usually needed in order to stabilize such drive systems. This paper first analyzes the system characteristics and the principles of existing active damping methods. Then a new voltage modulation based method named as "virtual positive impedance" method is introduced to guarantee the dc-link stability. This new approach is simple to apply and its implementation does not require the knowledge of system parameters and machine operating conditions. The proposed method is analyzed in details and verified by experiments.**

***Index Terms*—Active damping; small dc-link drive; stability; virtual positive impedance; voltage modulation**

## I. Introduction

ELECTROLYTIC capacitors are widely used in the commercial variable frequency inverters. However, the expected service lifetime at maximum rated conditions of the electrolytic capacitor is much lower than film capacitor, which motivates a replacement with film capacitor [1]-[3]. Investigations have shown that a smaller total capacitance will be sufficient for inverter applications by replacing electrolytic capacitors with film capacitors, and even the total volume of capacitor bank may be reduced [2]. Typically, drives equipped with film capacitors are applied in applications such as heating, ventilation and air-conditioning (HVAC), where the dynamic requirements for the motor shaft is moderate. Such drives are referred in the literature as small dc-link or slim dc-link drives [3]-[5].

Since the dc-link stage has the function to "stabilize" the rectified line voltage, instability of the dc-link voltage may occur when small dc-link drives are applied, especially when large grid inductances are present and this situation will be more critical for constant power load (CPL) conditions [3]-[13]. It is well-known that the CPL operation has the "negative impedance" characteristics [5]-[13]. When there is not enough damping effect in the grid and dc-link, it will result in a negative damping factor in the characteristic equation of the system [3]-[9], [12]-[13]. Due to the non-linear characteristics of the diode rectifier, the instability due to the negative damping is mainly present in the form of oscillations. This oscillation may result in overvoltage and shorten the lifetime of the power devices and the dc-link capacitors. Moreover, the oscillation components will also be present in the grid supply current and worsen the total harmonic distortion (THD) and the partially weighted harmonic distortion (PWHD). Thus, the oscillation components are required to be damped properly.

Various passive damping circuits, which are added to the dc-link, are investigated for dc-link stabilization [14]. However, the extra components will increase the physical size and the cost of the inverter, and the selection of the component ratings should be adjusted accordingly for different system ratings. Therefore, active damping control methods are preferred to stabilize the dc-link voltage in small dc-link drives, especially in HVAC applications with moderate shaft dynamic requirements. The basic idea is to achieve a positive system dynamic damping factor by controlling the actual power drawn by the machine from the dc-link [3]-[13]. It is straight forward to realize by controlling the torque reference current directly, normally by adding/injecting signals that are proportional to the dc-link voltage variation [6]-[10]. However, the common problem of the reference current control methods is that they are not able to work properly when the frequency of the variation part of the dc-link voltage exceeds the bandwidth of current control loop. Therefore, instead of controlling the current reference, methods based on reference voltage control are suggested [3]-[5], [11]-[13]. It is worthwhile to notice that

Manuscript received October 15, 2017; revised December 18, 2017; accepted January 16, 2018. Date of publication January xx, 2018; date of current version xx xx, 2018. This work was supported in part by Lodam A/S and in part by the PSO-ELFORSK Program. Recommended for publication by Editor xx xx. (*Corresponding author: Dong Wang.*)

The authors are with the Department of Energy Technology, Aalborg University, DK-9220 Aalborg, Denmark (e-mail: dwa@et.aau.dk; klu@et.aau.dk; por@et.aau.dk; lam@et.aau.dk; fya@et.aau.dk; fbl@et.aau.dk).

Color versions of one or more of the figures in this paper are available online at http://ieeexplore.ieee.org.

Digital Object Identifier

machine current/torque ripple may occur due to the imperfect dc-link voltage feedforward compensation caused by the time delay of the digital controller [15] and the current/voltage injection for achieving active damping control, and this is why small dc-link drives are mainly for the applications with moderate shaft dynamic requirements.

Nearly all the methods mentioned above [3]-[11] are introducing variation terms that are functions of the dc-link voltage variation in a proper way to guarantee that the system characteristic equation has a positive dynamic damping factor. The idea of introducing a virtual capacitor [8] or a virtual resistor [12] was proposed to explain the "physical" meaning behind these methods. However, a common disadvantage of these methods is that the introduced control parameters need to be tuned for different operating conditions and system parameters, which is not convenient. In this paper, a complete analysis of the small dc-link drive is firstly provided. The voltage drop caused by the commutation of the diode rectifier is considered in the system analysis. Its influence to the system performance is addressed. Then, the existing active damping methods are summarized by providing their general system characteristic equation, where the control parameter appears as an extra adding term and the choice of the parameter value required to stabilize the drive is system parameter and operating condition dependent. Moreover, the extraction methods of the dc-link voltage variation term are discussed. New extraction method by using an adaptive band-pass-filter (BPF) with the help of a frequency-locked loop (FLL) is suggested, where only necessary dc-link voltage variation term will be damped and operating conditions with "healthy" (stable) dc-link voltage, such as no-load or light load conditions, will not be affected by the active damping control. Thereafter, a new way to achieve a system positive dynamic damping factor, which changes the "negative impedance" characteristics of CPL operation to "virtual positive impedance" by voltage modulation, as briefly discussed in [16] by the authors, is elaborated and extended. The method is generalized by introducing two extra control parameters to fully control the reference dc-link voltage used in the space vector modulation (SVM). Superior to other methods, the introduced control parameters appear as gain factors (rather than an extra adding term) in the system characteristic equation. Thus, the system can simply be stabilized by controlling the sign of the control parameters, which does not require any knowledge of system parameters and/or operating conditions in implementation. The magnitudes of the control parameters control the magnitude of the system damping factor. Furthermore, its influence to the total duty cycle (or modulation index) of the two active vectors during each switching period is analyzed and over-modulation control is achieved. The strategy to determine the values of the control parameters is summarized, including optimal active damping control, minimization of total duty cycle variation, or both. At last, the experiment results are provided to validate the proposed methods and discussions regarding the influence of the proposed methods to the machine performance are given.

This paper is organized in the following manner. Section II describes the system modelling and the active damping control fundamentals. The general system characteristic equation of existing active damping solutions are summarized and provided. Then, the new voltage modulation based active damping method is analyzed in details in section III. Finally, the method is verified experimentally in section IV.

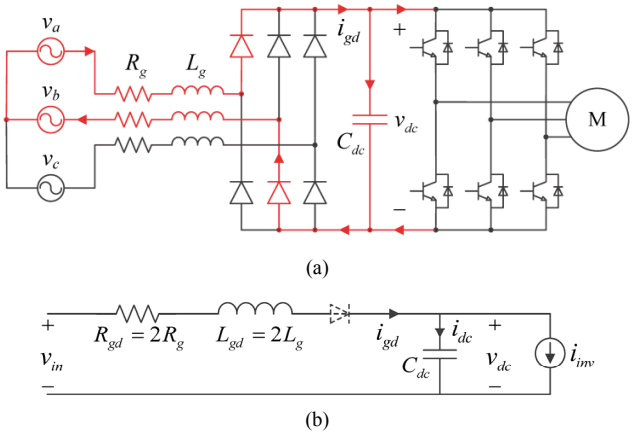


Fig. 1. System circuit diagram of a variable frequency drive. (a) Full bridge model. (b) Simplified model.

## II. Analysis of Small DC-Link Drive System

The characteristics of the small dc-link drive system and the concept of active damping methods are presented in this section.

### A. Analysis of Small DC-Link Drive

Fig. 1(a) illustrates the topology of widely used frequency converter with a front-end diode rectifier. The non-linear characteristics of the diodes and power switching devices make it complicated to analyze the characteristics of the circuit. Thus, the full bridge model is simplified and the equivalent system model is described as illustrated in Fig. 1(b).

When the current from grid side $i_{gd}$ in the dc-link is kept above zero, i.e. the whole rectifier is operating in continuous conduction mode and the presence of the diode can be neglected in the simplified model as shown in Fig. 1(b). The effect of the front-end diode rectifier can be taken into consideration by modifying the input voltage $v_{in}$ accordingly. When the effect of grid resistance ($R_g$) and inductance ($L_g$) can be neglected, the commutation period of the diode rectifier from one phase leg to the other is negligible and $v_{in}$ can be expressed as [3], [5], [17]:

$$v_{in}=\frac{3\sqrt{3}V_{ph}}{\pi}\left(1-\sum_{n=1}^{\infty}\frac{2}{(6n)^2-1}\cos(6n\omega_g t)\right), \quad (1)$$

where $V_{ph}$ is the amplitude of the grid phase voltage, and $\omega_g$ is the grid angular frequency. However, for situations that $R_g$ and $L_g$ cannot be neglected, e.g. weak grid with large $L_g$, the commutation period, where both three legs are conducting [17]-[18], cannot be neglected and $v_{in}$ cannot be solely represented by (1) any longer. The length of the commutation period is $L_g$ and $i_{gd}$ dependent, so as its influence to $v_{in}$ [17]. Such influence is represented by an equivalent non-ohmic resistance

$R_{Lg}$ in some literatures [3], [5], [9], [18]. This is acceptable when considering the influence on the dc component of $v_{in}$ only [18]. However, it is not suitable for the dynamic analysis, since $R_{Lg}$ does not exist physically and the presence of $R_{Lg}$ in the circuit will increase the system damping factor. During the commutation period, a voltage drop in $v_{in}$ will appear, This voltage difference $\Delta v_{in}$ can be expressed as [17]-[18]:

$$\Delta v_{in} = \sqrt{3}V_{ph}\left(\sin(\pi/3)-\sin(\pi/3+\omega_g t)\right),\ 0 \le t \le T_{cc}\,. \tag{2}$$

The commutation period $T_{cc}$ can be calculated as [17]-[18]:

$$T_{cc} = \frac{1}{\omega_g}\cos^{-1}\left(1-\frac{2\omega_g L_g}{\sqrt{3}V_{ph}}i_{gd}(t_{c0})\right), \tag{3}$$

where $i_{gd}(t_{c0})$ is the grid current at the initial time instant of the commutation. It can be seen that the value of $\Delta v_{in}$ is not $L_g$ and $i_{gd}$ dependent, however its existing time (commutation period) is $L_g$ and $i_{gd}$ dependent.

The inverter and the load are replaced by a current source, as shown in Fig. 1 (b), to perform as the load of the dc-link. The load current $i_{inv}$ can be controlled to perform different types of loads, such as resistive load, CPL, etc. When the motor draws a constant power $P_L$, the inverter current $i_{inv}$ can be expressed as [9], [12]:

$$i_{inv} = I_{inv} + \tilde{i}_{inv} = \frac{P_L}{v_{dc}} = \frac{P_L}{V_{dc}+\tilde{v}_{dc}} \cong \frac{P_L}{V_{dc}} - \frac{P_L}{V_{dc}^2}\tilde{v}_{dc}\,, \tag{4}$$

where $I_{inv}$ and $\tilde{i}_{inv}$ are the large and small signals of $i_{inv}$, $V_{dc}$ and $\tilde{v}_{dc}$ are the large and small signals of $v_{dc}$, respectively. The small signal impedance can be defined as:

$$Z_{inv} = \tilde{v}_{dc}/\tilde{i}_{inv} = -V_{dc}^2/P_L\,, \tag{5}$$

which is a negative value.

The state equations of the simplified system shown in Fig. 1 (b) can be expressed as:

$$L_{gd}\frac{di_{gd}}{dt} = v_{in} + \Delta v_{in} - R_{gd}i_{gd} - v_{dc} \tag{6}$$

$$C_{dc}\frac{dv_{dc}}{dt} = i_{gd} - i_{inv}\,. \tag{7}$$

The voltage drop $\Delta v_{in}$ is described by piecewise functions, i.e. zero voltage outside the commutation period, non-zero voltage during the commutation period as defined in (2). The above state equations should be solved for each piecewise, where the value of $\Delta v_{in}$ is not $L_g$ and $i_{gd}$ dependent.

By substituting (4) into (6) and (7), it can be obtained that:

$$\frac{d^2v_{dc}}{dt^2} + \left(\frac{R_{gd}}{L_{gd}} - \frac{P_L}{C_{dc}V_{dc}^2}\right)\frac{dv_{dc}}{dt} + \frac{1}{L_{gd}C_{dc}}\left(1-\frac{R_{gd}P_L}{V_{dc}^2}\right)v_{dc} = \frac{v_{in}+\Delta v_{in}}{L_{gd}C_{dc}} - \frac{2R_{gd}P_L}{L_{gd}C_{dc}V_{dc}}. \tag{8}$$

It can be seen that $\Delta v_{in}$ only appears in the right side of (8). Thus, it only influences the particular solution of (8). The values of $T_{cc}$ and $i_{gd}(t_{c0})$ only influence the initial value of the solution of each piecewise. The system stability is determined by the common solution of (8), which is not affected by $\Delta v_{in}$. The characteristic equation of the second order system in the Laplace domain can be obtained as:

$$s^2 + \underbrace{\left(\frac{R_{gd}}{L_{gd}} - \frac{P_L}{C_{dc}V_{dc}^2}\right)}_{a_{10}}s + \underbrace{\frac{1}{L_{gd}C_{dc}}\left(1-\frac{R_{gd}P_L}{V_{dc}^2}\right)}_{a_{20}} = 0\,. \tag{9}$$

According to Routh-Hurwitz stability criterion, the system is stable when $a_{10}$ and $a_{20}$ are greater than zero. Normally, $V_{dc}^2/P_L$ (representing the small signal impedance as (5)) is much greater than $R_{gd}$, i.e. $a_{20}$ is greater than zero. The system is stable if $a_{10}>0$, which is the condition for normal frequency converters with large electrolytic capacitors. However, it may be not true for small dc-link drives. When the criterion $a_{10}>0$ is not satisfied, the dc-link voltage and grid currents will become unstable or oscillating [6], [7], [12], and should be avoided. The resonant frequency of the oscillation can be estimated as:

$$\omega_0 = \sqrt{a_{20}} = \sqrt{\frac{1}{L_{gd}C_{dc}}\left(1-\frac{R_{gd}P_L}{V_{dc}^2}\right)} \approx \sqrt{\frac{1}{L_{gd}C_{dc}}}\,. \tag{10}$$

### *B. Principle of Active Damping Control*

To suppress the oscillation caused by the resonance between the inductors (including both grid side and dc-choke if there is any) and dc-link capacitors, it is straight forward to consider using the machine windings (i.e. inductors) as extra energy storage components to bypass part of the oscillating energy and therefore limit the oscillations [16]. This can be achieved by controlling the power drawn by the machine.

Taking the method from [9] as an example, a term proportional to the dc-link voltage variation term $\tilde{v}_{dc}$, i.e. the small signal of dc-link voltage, is added/injected to the torque producing current reference $i_q^*$, which can be expressed as:

$$i_q^* = I_q^* + \tilde{i}_q^* = I_q^* + g_{iq}\tilde{v}_{dc}\,. \tag{11}$$

where $I_q^*$ is the unmodified component, i.e. large signal of $i_q^*$ for steady state operating conditions, and $g_{iq}$ is the gain factor of $q$-axis injected current term. Similarly, a gain factor $g_{id}$ can be introduced to control the current injected to the $d$-axis.

It was supposed that the bandwidth of the current controller is sufficiently large, so that the small signal of the real current satisfies:

$$\tilde{i}_q \approx \tilde{i}_q^* = g_{iq}\tilde{v}_{dc}\,. \tag{12}$$

It is known that the instantaneous power drawn by the machine can be calculated as:

$$p_L = \frac{3}{2}(v_d i_d + v_q i_q)\,. \tag{13}$$

The influence of $\tilde{i}_q^*$ to $i_d$, which is caused by cross-saturation, is negligible since $\tilde{i}_q^*$ is small compared to $I_q^*$. Therefore, $i_{inv}$ can

be linearized at $V_{dc}$ when $\tilde{v}_{dc}/V_{dc}$ approaches zero:

$$i_{inv}=\frac{p_L}{v_{dc}}=\frac{3}{2}\left((V_d-\omega_0 L_q\tilde{i}_q)I_d+V_q(I_q+\tilde{i}_q)\right)\frac{1}{V_{dc}+\tilde{v}_{dc}}$$
$$\approx\frac{P_L}{V_{dc}}+(\frac{3}{2}\frac{(V_q-\omega_0 L_q I_d)g_{iq}}{V_{dc}}-\frac{P_L}{V_{dc}^2})\tilde{v}_{dc}\triangleq\frac{P_L}{V_{dc}}+(g-\frac{P_L}{V_{dc}^2})\tilde{v}_{dc}\quad(14)$$

The frequency of the small signals $\omega_0$ can be estimated by (10).

By substituting (14) into (6) and (7), it can be obtained that:

$$s^2+\underbrace{\left(\frac{R_{gd}}{L_{gd}}+\frac{g-P_L/V_{dc}^2}{C_{dc}}\right)}_{a_{11}}s+\underbrace{\frac{1}{L_{gd}C_{dc}}\left(1+R_{gd}(g-\frac{P_L}{V_{dc}^2})\right)}_{a_{21}}=0\ .\quad(15)$$

Compared with (4) and (9), a new term $g$ (defined in (14)) is introduced in (15) by injecting a variation term $\tilde{i}_q^*$. It can easily be found that when

$$g\geq P_L/V_{dc}^2\ ,\quad(16)$$

$a_{11}$ and $a_{21}$ will be greater than zero and the system is stable. The required minimum gain factor $g_{iq}$ that is directly used in the controller as (12) can then be obtained according to its relationship to factor $g$ as given in (14). It can be found that $g_{iq}$ is system parameter and operation condition dependent. A similar criterion can be obtained by repeating the above analysis when injecting into the $d$-axis current reference.

In a real digital control system, the bandwidth of the current loop is limited and the condition to achieve (12) can hardly be satisfied. Therefore, instead of controlling the current reference, active damping methods based on the reference voltage control are suggested [3]-[5], [11]-[13].

Similar to the above current injection method, voltage variation terms $\tilde{v}_d$ and $\tilde{v}_q$ are injected into the machine $d$- and $q$-axes stator voltages to achieve positive dynamic damping coefficient. The voltage variations terms are defined as [3]:

$$\tilde{v}_d=g_{vd}\tilde{v}_{dc}\ \text{ and }\ \tilde{v}_q=g_{vq}\tilde{v}_{dc}\ ,\quad(17)$$

where $g_{vd}$ and $g_{vq}$ are the gain factors of $d$- and $q$-axes injected voltage terms, respectively.

Similar to (14), $i_{inv}$ can be approximated as:

$$i_{inv}=\frac{p_L}{v_{dc}}\approx\frac{3}{2}\left((V_d+\tilde{v}_d)I_d+(V_q+\tilde{v}_q)I_q\right)\frac{1}{V_{dc}+\tilde{v}_{dc}}$$
$$\approx\frac{P_L}{V_{dc}}+(\frac{3}{2}\frac{I_d g_{vd}+I_q g_{vq}}{V_{dc}}-\frac{P_L}{V_{dc}^2})\tilde{v}_{dc}\triangleq\frac{P_L}{V_{dc}}+(g-\frac{P_L}{V_{dc}^2})\tilde{v}_{dc}\quad(18)$$

It can be observed that (18) has the same pattern as (14). The system characteristic equation identical to (15) can be obtained. Stability criterion same as (16) would be achieved and suitable gain factors $g_{vd}$ and $g_{vq}$ can then be determined accordingly.

It can be found that existing studies have mainly focused on the way of achieving dynamic positive system damping factors by injecting extra current/voltage variation terms into the drive system [3]-[12], i.e. by adding extra terms in $a_{11}$ and $a_{21}$ to make them positive values. The minimum gain factors in (12) and (17) used in the controller need to be carefully determined and they are affected by the system parameters and/or machine operating conditions.

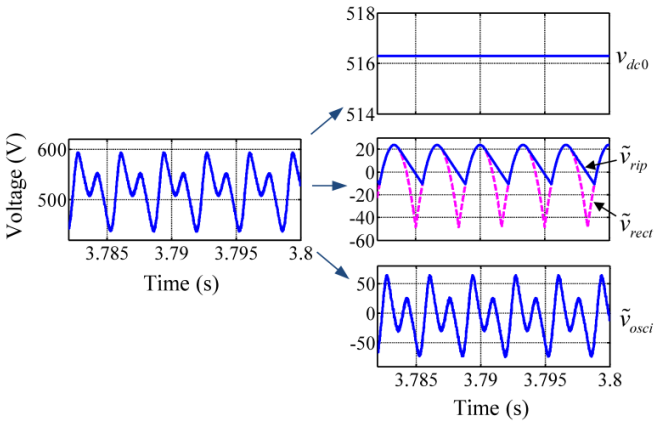


Fig. 2. Composition of the dc-link voltage. (a) Small dc-link voltage $v_{dc}$. (b) Top: dc part $v_{dc0}$; middle: dc-link ripple voltage $\tilde{v}_{rip}$, and rectified component $\tilde{v}_{reci}$; bottom: dc-link voltage oscillating term $\tilde{v}_{osci}$.

### C. DC-Link Voltage Variation Extraction

The dc-link voltage variation, i.e. the small signal of the dc-link voltage $\tilde{v}_{dc}$ caused by the resonance between $C_{dc}$ and $L_{gd}$, is required to perform active damping control to the small dc-link drive system. It can be seen from Fig. 2 that the dc-link voltage would contain three parts: the dc part ($v_{dc0}$), the ripple voltage ($\tilde{v}_{rip}$), and the oscillating term ($\tilde{v}_{osci}$). Regarding the input of the diode rectifier, the source voltage contains both the dc part ($v_{dc0}$) and the rectified component ($\tilde{v}_{rect}$) as described in (1). The presence of the dc-link will smoothen the rectified component ($\tilde{v}_{rect}$) to the ripple component ($\tilde{v}_{rip}$) as shown in Fig. 2(b). For a small dc-link drive, $\tilde{v}_{rip}$ will degenerate to $\tilde{v}_{rect}$ rapidly as the load increases. Fig. 2(a) shows the small dc-link voltage with $C_{dc}=14\,\mu\text{F}$ and $L_g=1.86\,\text{mH}$. The resonant frequency is 697 Hz according to (10). Thus the oscillating term $\tilde{v}_{osci}$ contains mainly 600 Hz component (for 50 Hz grid frequency) as shown in Fig. 2(b), which is the frequency of the second harmonic of $\tilde{v}_{rect}$.

There could briefly be two ways to define the small signal $\tilde{v}_{dc}$ that will be used for active damping control: including $\tilde{v}_{rip}$ or not. When $\tilde{v}_{rip}$ is included in $\tilde{v}_{dc}$, the large signal $V_{dc}$ only contains the dc component ($v_{dc0}$) and can simply be obtained by using a low-pass-filter (LPF). However, since $\tilde{v}_{rip}$ is included in $\tilde{v}_{dc}$, the active damping control will try to damp it as well. For machine drive systems, this will result in large machine current ripple at rectified frequency (300 Hz for 50 Hz grid). Large torque ripple at the same frequency will be generated, which may reduce the bearing lifetime and increase the machine losses and noise level. Therefore, instead of damping both $\tilde{v}_{rip}$ and $\tilde{v}_{osci}$, it could be a better choice to damp $\tilde{v}_{osci}$ only, i.e. excluding $\tilde{v}_{rip}$ from $\tilde{v}_{dc}$.

It is not straightforward when obtaining $\tilde{v}_{rip}$ from $v_{dc}$. However, due to the fact that $\tilde{v}_{rip}$ approaches $\tilde{v}_{rect}$ rapidly as the load increases for small dc-link drive, $\tilde{v}_{rect}$ was used to represent $\tilde{v}_{rip}$

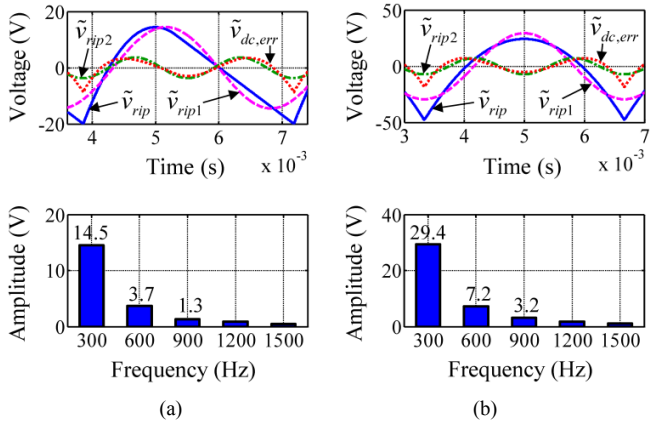


Fig. 3. Signal and spectrum of dc-link ripple voltage $\tilde{v}_{rip}$ and its harmonic components. (a) Very light load condition. (b) Heavy load condition.

in many existing studies and several methods have been proposed to estimate $\tilde{v}_{rect}$ (or $V_{rect} = v_{dc0} + \tilde{v}_{rect}$). In [12], a Luenberger-type source state estimator is built to estimate $V_{rect}$. However, besides the parameters of the small dc-link drive (e.g. $C_{dc}$), the parameters of the grid (e.g. $L_{gd}$) are required as well to build the state equations and to tune the introduced gain matrix correctly, which makes this method is not easy to implement in applications and estimation error exists as well [12]. In [13], a method based on phase-locked loop (PLL) and frequency-locked loop (FLL) trackers is introduced, which can calculate $V_{rect}$ from $v_{dc}$ by identifying the amplitude, frequency, and phase angle of $V_{rect}$. However, both the above methods may fail to estimate the large signal $V_{dc}$ correctly at no load or very light load conditions, where the rectifier is no longer operating in continuous conduction mode and $\tilde{v}_{rip}$ cannot be represented by $\tilde{v}_{rect}$ anymore.

An alternative method is to use the fundamental component of $\tilde{v}_{rip}$, which is a pure sinusoidal signal at the rectified frequency ($6\omega_g$), to approximate $\tilde{v}_{rip}$ [16]. This fundamental component $\tilde{v}_{rip1}$ can simply be obtained by using a band-pass-filter (BPF), such as a non-ideal proportional-resonant (PR) controller [19]. The above mentioned approximation will introduce an error signal $\tilde{v}_{dc,err}$, which mainly contains the second order harmonic $\tilde{v}_{rip2}$ as shown in Fig. 3. The error is small and it is acceptable.

Moreover, it is worth to note that the rectified frequency ($6\omega_g$) is required as the center frequency of the BPF. In order to achieve a general and robust drive system, the FLL in [13] is adopted to detect the real rectified frequency based on the measured dc-link voltage $v_{dc}$ to achieve an adaptive BPF, so that the possible phase shift caused by grid frequency drift can be minimized when extracting $\tilde{v}_{rip1}$. Fig. 4 shows the performance of the FLL. It can be seen that the detected rectified frequency can follow the reference well, where the frequency of the three-phase power supply changes from 94% to 106% of 50 Hz, i.e. rectified frequency changes from 282 Hz to 318 Hz. The frequency error is about 0.2 Hz for 282 Hz. A PR controller with a quality factor of five is used to perform as a BPF. The phase shift around the center frequency (i.e. around 300 Hz) is about one degree per Hz. Thus, the phase shift is very small and

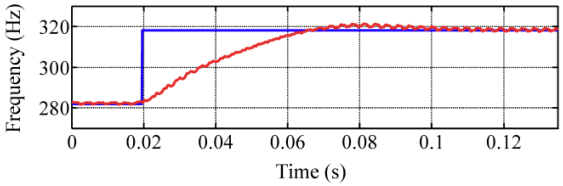


Fig. 4. FLL tracking performance for a frequency step change. Blue curve: reference frequency; red curve: estimated frequency by the FLL algorithm.

negligible. Compared with the above methods in [12] and [13], using an adaptive BPF is easy to implement without the requirement of system parameters and can work properly in various operating conditions.

Furthermore, regarding the conditions where $\tilde{v}_{rip}$ can be represented by $\tilde{v}_{rect}$, $\tilde{v}_{rect}$ can be approximated according to (1) after $\tilde{v}_{rip1}$ has been obtained from the BPF. For example, $\tilde{v}_{rip2}$ can be calculated as:

$$\begin{aligned}\tilde{v}_{rip2} &= c_2 \cos(12\omega_g t) = c_2\left(2\cos^2(6\omega_g t) - 1\right) \\ &= c_2\left(2\left(\tilde{v}_{rip1}/c_1\right)^2 - 1\right),\end{aligned} \tag{19}$$

where $c_n$ is the coefficient of $\cos(6n\omega_g t)$ as defined in (1). As more components $\tilde{v}_{ripn}$ are included, the more accurate $\tilde{v}_{rect}$ can be approximated. However, using $\tilde{v}_{rip1}$ to represent $\tilde{v}_{rect}$ is recommended, because:

1. The amplitude of $\tilde{v}_{rip2}$ is 7.2 V for 515 V dc-link (no load condition for 220 V grid phase voltage), which is only 1.4%. Thus, $\tilde{v}_{rip1}$ should be good enough.
2. No extra calculations are needed.
3. The above estimation in (19) has the same problem as the methods in [12] and [13], i.e. it is only valid for conditions where $\tilde{v}_{rip}$ approaches $\tilde{v}_{rect}$.

## III. Proposed Voltage Modulation Based Active Damping Method

Instead of achieving dynamic positive system damping factors by injecting extra current/voltage variation terms with proper gain factors, the problem may be solved by another method – changing the negative impedance $Z_{inv}$ (as defined in (5)) to a positive value. For example, by simply reversing the sign of $\tilde{v}_{dc}$ in (5), the impedance could "change" from negative to positive. This reversing action changes the reference dc-link voltage signal $v_{dc}^*$ as illustrated in Fig. 5. The reconstructed dc-link voltage signal (Fig. 5(c)) is further used to determine the duty-cycles from the voltage commands when performing SVM.

It is worth to notice that the natural behavior/characteristics of the inverter with CPL cannot be really changed from the negative impedance to the positive impedance. The essential idea of the proposed method is still to control the instantaneous power drawn by the machine. Thus, the inverter is no longer facing a CPL, but a varying power load that contains both the CPL and an extra oscillating component proportional to $\tilde{v}_{dc}$. The mathematical prove for achieving this important characteristic by simply reserving the sign of $\tilde{v}_{dc}$ is given below.

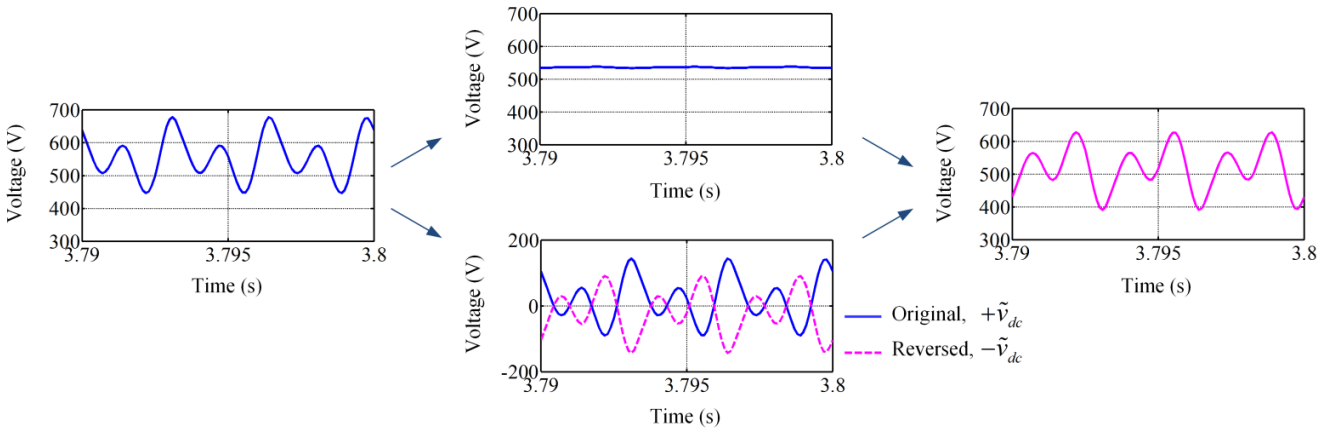


Fig. 5. Decomposing and reconstruction of reference dc-link voltage signal $v_{dc}^*$. (a) dc-link voltage $v_{dc}$. (b) from top to bottom: large signal ($V_{dc}$), small signal $\tilde{v}_{dc}$ and reversed $\tilde{v}_{dc}$. (c) reconstructed $v_{dc}^*$ with $V_{dc}$ and reversed $\tilde{v}_{dc}$.

The load power $P_L$ can be calculated by the vector scalar product as:

$$P_L = \overline{v}_{abc} \cdot \overline{i}_{abc}, \tag{20}$$

where $\overline{v}_{abc}$ and $\overline{i}_{abc}$ are machine voltage and current vectors.

When the reference dc-link voltage signal $v_{dc}^*$ is reconstructed from $V_{dc}+\tilde{v}_{dc}$ to $V_{dc}-\tilde{v}_{dc}$ as shown in Fig. 5, the output voltage vector becomes $\overline{v}_{abc,rec}$ instead of $\overline{v}_{abc}$, which can be calculated as:

$$\overline{v}_{abc,rec} = \frac{\overline{v}_{abc}}{v_{dc}^*} v_{dc} = \overline{v}_{abc} \frac{V_{dc}+\tilde{v}_{dc}}{V_{dc}-\tilde{v}_{dc}}, \tag{21}$$

Then the load power becomes $P_{L,rec}$ instead of $P_L$:

$$P_{L,rec} = \overline{v}_{abc,rec} \cdot \overline{i}_{abc} = \frac{V_{dc}+\tilde{v}_{dc}}{V_{dc}-\tilde{v}_{dc}} \overline{v}_{abc} \cdot \overline{i}_{abc} = P_L \frac{V_{dc}+\tilde{v}_{dc}}{V_{dc}-\tilde{v}_{dc}}, \tag{22}$$

The inverter current $i_{inv}$ at load $P_{L,rec}$ can be calculated as:

$$i_{inv} = I_{inv} + \tilde{i}_{inv} = \frac{P_{L,rec}}{v_{dc}} = \frac{P_L}{V_{dc}-\tilde{v}_{dc}} \approx \frac{P_L}{V_{dc}} + \frac{P_L}{V_{dc}^2}\tilde{v}_{dc}. \tag{23}$$

Compared with (4), it can be seen that (23) has the same pattern but the sign of $\tilde{v}_{dc}$ term is reversed. The impedance of the inverter with load $P_{L,rec}$ now becomes positive. The system characteristic equation becomes:

$$s^2 + \underbrace{\left(\frac{R_{gd}}{L_{gd}} + \frac{P_L}{C_{dc}V_{dc}^2}\right)}_{a_{12}} s + \underbrace{\frac{1}{L_{gd}C_{dc}}\left(1+\frac{R_{gd}P_L}{V_{dc}^2}\right)}_{a_{22}} = 0. \tag{24}$$

The coefficients $a_{12}$ and $a_{22}$ are now always larger than zero and the system is always stable. Therefore, the system can be stabilized by simply reversing the sign of $\tilde{v}_{dc}$ in the extracted reference dc-link voltage signal, and a "virtual positive impedance" of the system can be obtained.

The "virtual positive impedance" concept can be further generalized by introducing gain factors $k_{v0}$ and $k_v$ for controlling the dc deviations and variation components of the reconstructed $v_{dc}^*$ from $v_{dc}$ respectively. The reconstructed dc-link reference voltage can be expressed as $v_{dc}^* = k_{v0}V_{dc} - k_v\tilde{v}_{dc}$. It can then be obtained that:

$$i_{inv} = I_{inv} + \tilde{i}_{inv} \approx \frac{P_L}{k_{v0}V_{dc}} + \frac{k_v P_L}{k_{v0}^2 V_{dc}^2}\tilde{v}_{dc} \tag{25}$$

$$s^2 + \underbrace{\left(\frac{R_{gd}}{L_{gd}} + \frac{k_v P_L}{C_{dc}k_{v0}^2V_{dc}^2}\right)}_{a_{13}} s + \underbrace{\frac{1}{L_{gd}C_{dc}}\left(1+\frac{k_v R_{gd}P_L}{k_{v0}^2V_{dc}^2}\right)}_{a_{23}} = 0. \tag{26}$$

According to Routh-Hurwitz stability criterion, it can be found that:

1. When $k_v \geq 0$, the coefficients $a_{13}$ and $a_{23}$ are always greater than zero, and the system is always stable.
2. $k_v=0$ (i.e. $v_{dc}^*=V_{dc}$) is already sufficient to stabilize the system.
3. $k_{v0}=k_v=1$ represent the condition illustrated in Fig. 5.
4. Increasing $k_v$ can increase $a_{13}$ and $a_{23}$, and thus increasing the damping effect, so that the variation parts such as $\tilde{v}_{dc}$ can be suppressed further. But the machine performance might be sacrificed when too much oscillating energy is injected into the machine.
5. When $k_v=-1$, i.e. $\tilde{v}_{dc}$ is not reversed and a negative impedance is present, the increase of $k_{v0}$ will increase $a_{13}$ and the system can be stabilized till $a_{13}>0$. However, the determination of $k_{v0}$ requires the knowledge of system parameters and operation conditions, which is not convenient in the implementation. Furthermore, $a_{13}$ is always smaller than $R_{gd}/L_{gd}$ no matter how large $k_{v0}$ is, which means the maximum damping factor is limited.
6. When $k_v \geq 0$, reducing $k_{v0}$ will increase $a_{13}$, and thus increasing the damping effect to $\tilde{v}_{dc}$. However, it will result in the situation that the large signals of the commanded reference voltages are lower than that of the real machine voltages, which would cause difficulties when applying state observers to estimate e.g. machine flux linkage, speed and position.

Considering the limitations discussed above in items 5 and 6, it is recommended to achieve active damping control by manipulating $k_v$, while keeping $k_{v0}$ to one.

### A. Over-modulation Control

When the dc-link voltage is varying and used in the SVM, over-modulation may occur for rated machine voltage outputs. The situation when the machine voltage vector is located in the middle of each 60° section during the SVM is considered as the worst case, since the required total duty cycle of the two active vectors during each switching period reaches its maximum at this position. When there is no active damping method implemented, the total duty cycle $D_0$ can be calculated and linearized as:

$$D_0^2 = \left( \frac{\left|\overline{v}_{dq}\right|}{v_{dc}/\sqrt{3}} \right)^2 \approx 3(v_d^2 + v_q^2)\left( \frac{1}{V_{dc}^2} - \frac{2}{V_{dc}^3}\tilde{v}_{dc} \right) = A - \frac{2A}{V_{dc}}\tilde{v}_{dc}, \quad (27)$$

where $A=3(v_d^2+v_q^2)/V_{dc}^2$. The total duty cycle varies as dc-link voltage varies for a fixed output voltage, due to the oscillation term $\tilde{v}_{dc}$. When the amplitude of the machine voltage vector is high, over-modulation may occur when the varying $v_{dc}$ reaches its local minimums. The maximum allowable amplitude of the machine voltage vector will then be sacrificed.

For the "virtual positive impedance" method, the voltage vector in the rotor reference frame under the reconstructed $v_{dc}^*$ can be expressed and linearized as:

$$\overline{v}_{dq1} = \mathbf{P}\cdot\overline{v}_{abc,rec} \approx \frac{\overline{v}_{dq}}{k_{v0}}\left( 1 + \frac{k_{v0}+k_v}{k_{v0}V_{dc}}\tilde{v}_{dc} \right), \quad (28)$$

where $\mathbf{P}$ is the $dq$ transformation matrix.

To simplify the analysis, let $k_{v0}=1$ according to the previous recommendation. The total duty cycle $D_1$ under the active damping control can be calculated and linearized as

$$D_1^2 = \left( \frac{\left|\overline{v}_{dq1}\right|}{v_{dc}/\sqrt{3}} \right)^2 = D_0^2\left( 1 + \frac{1+k_v}{V_{dc}}\tilde{v}_{dc} \right)^2 \approx A + \frac{2A}{V_{dc}}k_v\tilde{v}_{dc}. \quad (29)$$

It can be observed that:

1. when $k_v=0$ (i.e. $v_{dc}^*=V_{dc}$), the total duty cycle is not influenced by the real dc-link voltage, which is obvious;
2. when $k_v=1$, the variation term in (29) has opposite sign of that in (27). $\tilde{v}_{dc}$ has normally a symmetrical positive and negative periods; but the peak value of $\tilde{v}_{dc}$ in (29) is reduced due to active damping control and it results in a reduced maximum duty cycle for (29).

Therefore, it is easy for the voltage modulation based "virtual positive impedance" method to control the variation of the total duty cycle, and achieve the active damping control without sacrificing the maximum allowable amplitude of the machine voltage vector. The value of the gain factor $k_v$ has clear meanings:

1. $k_v\geq 0$ to achieve active damping; the larger the value of $k_v$, the larger the value of the "virtual positive impedance" and the more damping effects;
2. $k_v=0$ to reduce the over-modulation caused by varying dc-link voltage; increasing $k_v$ will increase the over-modulation range; $k_v=1$ has smaller over-modulation range than that experienced in the situation of no active damping.

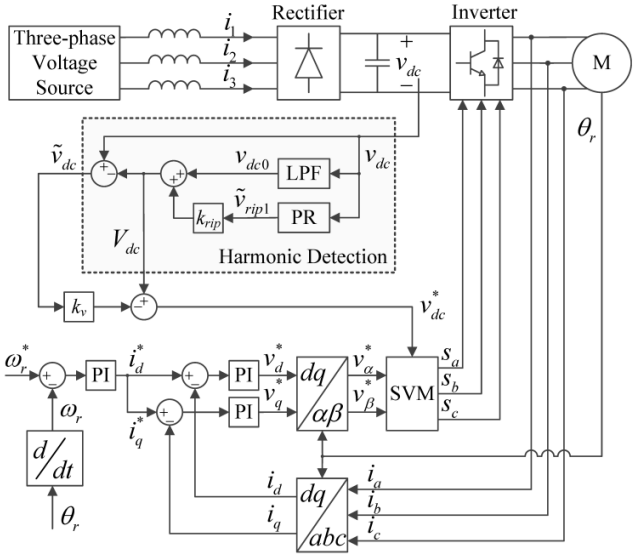


Fig. 6. System block diagram of small dc-link SynRM drive with "virtual positive impedance" active damping method and field-oriented-control.

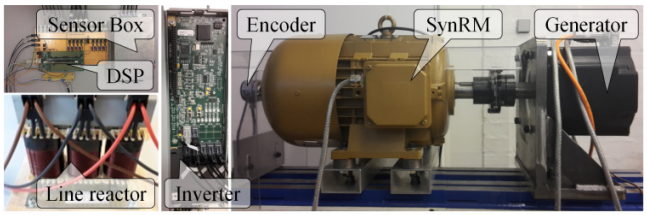


Fig. 7. Picture of the test setup of small dc-link SynRM drive.

TABLE I
MOTOR PARAMETERS

| Synchronous Reluctance Machine | | | |
|---|---|---|---|
| Rated power | 5.5 kW | Rated frequency | 50 Hz |
| Rated voltage | 353 V | Power factor | 0.69 |
| Rated current | 13.9 A | Stator resistance | 0.38 Ω |
| Rated speed | 1500 rpm | Inertia | $1.9\times10^{-2}$ kg·m$^2$ |
| Rated torque | 35.0 N·m | Pole pairs | 2 |

It should be noted that $\tilde{v}_{dc}$ decreases as $k_v$ increases. The amplitude of the equivalent injected voltage term (28) will have a "saturated" value. Thus, infinite $k_v$ will not help too much in the active damping control. In contrast, it may cause large transient or even stability problem when the dc-link voltage faces a sudden change, e.g. at step load condition. It can be seen in the experimental verification part that the oscillation terms can already be effectively damped when $k_v=2$.

## IV. EXPERIMENTAL VERIFICATIONS

The system topology to investigate the proposed "virtual positive impedance" active damping method is illustrated in Fig. 6. It can be seen that the dc component $v_{dc0}$ is obtained by using a LPF. The component at the rectifier frequency $\tilde{v}_{rip1}$,

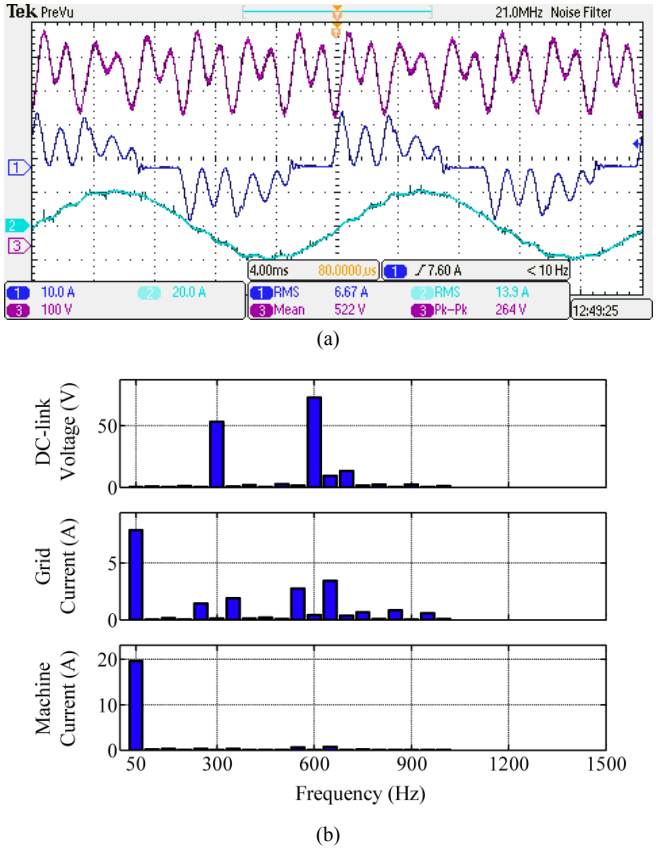


Fig. 8. Experimental results at 1500 rpm 13.9 A load without active damping control. (a) Waveforms, top: dc-link voltage; middle: grid current; bottom: machine current. (b) Spectrum from 50 Hz to 900 Hz.

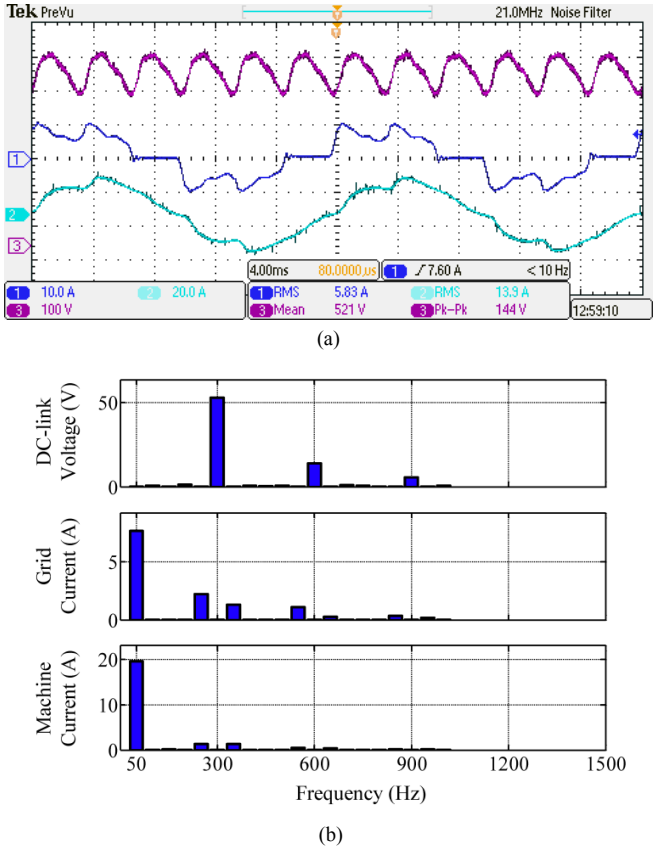


Fig. 9. Experimental results of active damping control with $k_{rip}$=0 and $k_v$=1 at 1500 rpm 13.9 A load. (a) Waveforms, top: dc-link voltage; middle: grid current; bottom: machine current. (b) Spectrum from 50 Hz to 900 Hz.

which is 300 Hz for 50 Hz grid, is obtained by using a PR controller as discussed in section II.C, and $k_{rip}$ is used to control whether $\tilde{v}_{rip1}$ should be included in the small signal $\tilde{v}_{dc}$ or not.

Fig. 7 shows the experimental platform. The small dc-link drive mainly includes a modified 7.5 kW converter and a 5.5 kW SynRM. A 14 µF film capacitor has been mounted to serve as the dc-link. A three-phase line reactor is used to simulate the soft grid, and the input phase inductance is estimated to be 1.86 mH. The converter parameters are the same with those in section II.C. Thus, for 388 V, 50 Hz grid, the oscillating term $\tilde{v}_{osci}$ contains mainly a 600 Hz component. The parameters of the SynRM are given in Table I.

Fig. 8 shows the performance of the small dc-link drive at machine rated operating condition (13.9 A load at 1500 rpm) when no active damping control is applied. It can be seen that there is a 600 Hz oscillation term in the dc-link voltage as well as 550 Hz and 650 Hz terms in the grid current. The grid current THD and PWHD are 66.0% and 74.3% respectively, which are high and not acceptable. Damping methods are required to stabilize the dc-link voltage and reduce the harmonics in the grid current.

Fig. 9 and Fig. 10 shows the experimental results of the proposed active damping control at 1500 rpm 13.9 A load with two selected control configurations. The performance of the "virtual positive impedance" active damping control (as illustrated in Fig. 5) is shown in Fig. 9. Compared with the performance without active damping (as shown in Fig. 8), it can be seen that the voltage and current oscillations caused by the resonance are greatly damped. The grid current THD is reduced from 66.0% to 37.3% and the PWHD is reduced from 74.3% to 34.0%. The machine current THD is increased from 5.3% to 10.5%, mainly due to the presence of 300±50 Hz terms caused by the intention of damping $\tilde{v}_{rip}$ in the dc-link voltage.

As discussed in section III, the oscillations can be further damped by increasing the gain factor $k_v$. Fig. 10 shows the performance of the proposed method with $k_{rip}$=1 and $k_v$=2. The grid current THD and the PWHD values are reduced to 39.5% and 41.4% respectively. The machine current THD is reduced to 4.8% even for higher $k_v$ value since $\tilde{v}_{rip1}$ is excluded from $\tilde{v}_{dc}$.

Tests were carried out with different control configurations. Table II summarizes the steady state performance of the "virtual positive impedance" active damping control with different control configurations when the machine is operating at 1500 rpm 13.9 A load. It can be seen that when constant $V_{dc}$ ($k_{rip}$=0 and $k_v$=0) is used to serve as reference dc-link voltage in the SVM, the oscillations can be damped already, which validates the discussions given in section III. When $k_{rip}$ = 0 i.e. $\tilde{v}_{rip}$ is included in $\tilde{v}_{dc}$, the machine current THD increases to 10.5% with the active damping control of $k_v$=1. While for $k_{rip}$=1, the machine current THD reduces to 4.2% for the same damping gain factor. Thus, from the machine performance point of view, it is highly recommended not to compensate $\tilde{v}_{rip}$. An appropri-

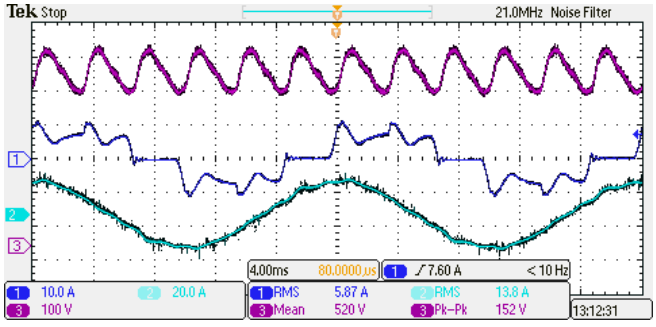


(a)

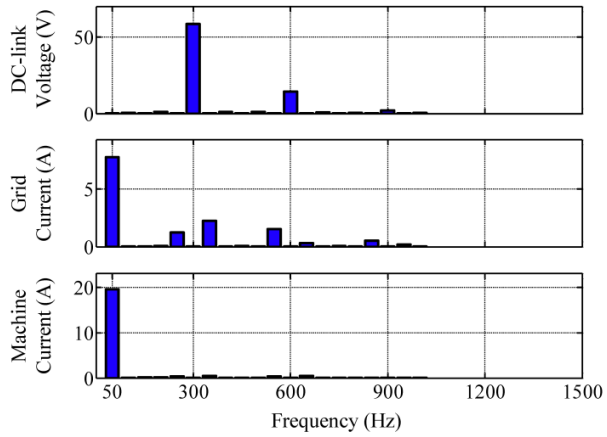


(b)

Fig. 10. Experimental results of active damping control with $k_{rip}$=1 and $k_v$=2 at 1500 rpm 13.9 A load. (a) Waveforms, top: dc-link voltage; middle: grid current; bottom: machine current. (b) Spectrum from 50 Hz to 900 Hz.

TABLE II
ACTIVE DAMPING CONTROL PERFORMANCE AT 1500RPM 13.9A LOAD

| Control configurations | $v_{dc}$ variation [a] (V) | $V_{dc300}$ [b] (V) | $V_{dc600}$ [c] (V) | Grid current THD | Grid current PWHD | Machine current THD |
|---|---|---|---|---|---|---|
| No damping | 252 | 53.3 | 72.6 | 66.0% | 74.3% | 5.3% |
| $k_{rip}=0$, $k_v=0$ | 147 | 53.1 | 29.0 | 40.4% | 39.3% | 6.4% |
| $k_{rip}=0$, $k_v=1$ | 118 | 53.1 | 14.0 | 37.3% | 34.0% | 10.5% |
| $k_{rip}=1$, $k_v=0$ | 160 | 56.8 | 33.4 | 44.2% | 46.5% | 3.9% |
| $k_{rip}=1$, $k_v=1$ | 135 | 57.8 | 19.9 | 40.6% | 43.4% | 4.2% |
| $k_{rip}=1$, $k_v=2$ | 126 | 58.4 | 14.5 | 39.5% | 41.4% | 4.8% |

[a] Peak-to-peak value of the voltage variation term $\tilde{v}_{dc}$
[b] Amplitude of 300 Hz component of $\tilde{v}_{dc}$
[c] Amplitude of 600 Hz component of $\tilde{v}_{dc}$

ate estimation of $\tilde{v}_{rip}$ is important as discussed in section II.C. The oscillations caused by the resonance can be further damped by increasing the value of $k_v$ if lower grid current THD and PWHD are expected.

Furthermore, it can be seen that the machine current THD is even lower when only the oscillation term of the dc-link voltage (i.e. 600 Hz component) is damped compared with the performance when no active damping control is applied. This is because that the measured dc-link voltage used in the SVM calculation is different with the dc-link voltage at the inverter voltage output time instant, which is due to the time delay caused by the digital controller [15]. Such imperfect dc-link voltage feedforward compensation will be amplified by the

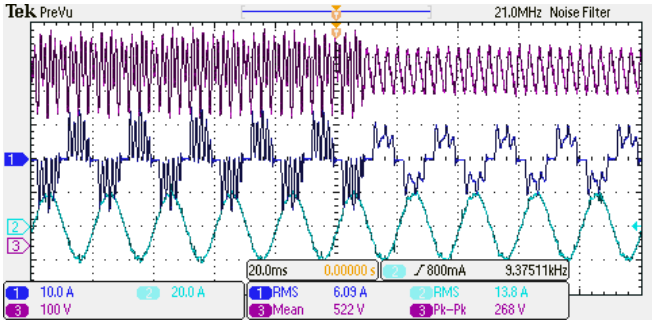


Fig. 11. Experimental result of the transient performance when enabling the active damping control ($k_{rip}$=1 and $k_v$=2) on-line at 1500 rpm 13.9 A load condition. Waveforms, top: dc-link voltage; middle: grid current; bottom: machine current.

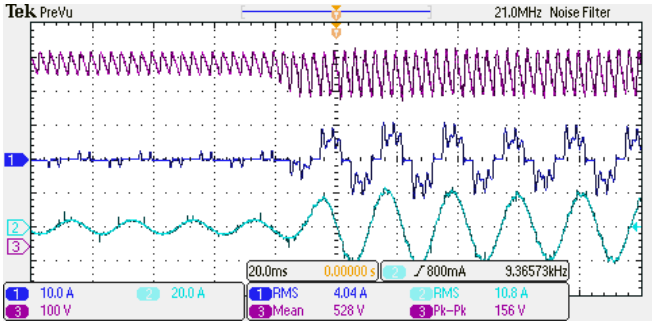


(a)

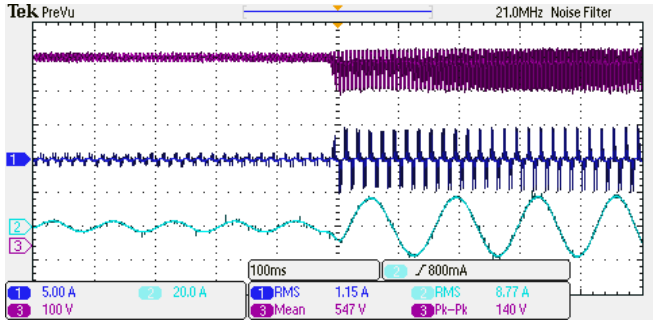


(b)

Fig. 12. Experimental results at step load (from no-load to 13.9 A load) conditions with active damping control ($k_{rip}$=1 and $k_v$=2). Waveforms, top: dc-link voltage; middle: grid current; bottom: machine current. (a) At 1500 rpm. (b) At 300 rpm.

large dc-link voltage oscillation term and result in high machine current ripples. The damped dc-link voltage oscillation term will help to reduce the machine current ripples to achieve even better machine performance.

Besides the steady state performance of the proposed "virtual positive impedance" active damping control, the system transient performance at selected operating conditions are shown in Fig. 11 and Fig. 12 to illustrate that the proposed active damping technique is able to handle various operating conditions properly. Fig. 11 shows the system transient performance when enabling the active damping control ($k_{rip}$=1 and $k_v$=2) on-line at 1500 rpm 13.9 A load condition. It can be seen the proposed active damping method can damp the dc-link voltage fast and effectively without generating additional large transi-

ent. Fig. 12 shows the system transient performance under load step change condition (from no-load to 13.9 A load) at 1500 rpm and 300 rpm respectively, when active damping control ($k_{rip}$=1 and $k_v$=2) is enabled. It can be seen that the proposed active damping method can handle the step load change well without generating additional large transient. Moreover, it is worth noting that the dc-link voltage variation term $\tilde{v}_{rip}$ is small at no-load conditions and it increases to $\tilde{v}_{rect}$ as load increases (as discussed in section II.C Fig. 2). The proposed dc-link voltage variation extraction method will use a signal close to $\tilde{v}_{rip}$ rather than $\tilde{v}_{rect}$ for dc-link voltage variation extraction as illustrated in section II.C Fig. 3. Thus, the dc-link voltage at "healthy" (stable) operating conditions will not be affected, and the machine current will not be distorted since the dc-link voltage under this condition is not forced to be compensated to a signal close to $\tilde{v}_{rect}$ with the proposed active damping technique.

## V. Conclusion

In this paper, the characteristics of the small dc-link drive system are analyzed and the concept of system active damping control is summarized. The extraction of the dc-link voltage variation term, which is one of the key steps in implementing active damping control, is discussed in details. A new method is proposed to estimate the rectified voltage term, which is based on its fundamental component obtained by simply using an adaptive BPF (e.g. PR controller) with the help of a PLL. It is recommended to approximate the dc-link ripple voltage by its fundamental component, which is suitable for various operating conditions and can provide satisfactory results.

More importantly, a new way to stabilize the small dc-link drive system, which has been named as "virtual positive impedance" method, is introduced and verified. This method ensures the system stability without the need of obtaining the compensation factors dynamically according to the system parameters and operating conditions. The damping effects can be controlled by simply introducing a gain factor to the voltage variation term. The experimental results show that with the proposed method and the gain factor set to two, the grid current THD has been reduced from 66.0% to 39.5% and the PWHD from 74.3% to 41.4%, even with the extra benefit that the motor current THD has been reduced from 5.3% to 4.8%. Moreover, the analysis of the voltage modulation based "virtual positive impedance" active damping method shows that it can provide an easy control to the variation of the total duty cycle caused by the varying dc-link voltage. Thus, it is possible to limit or even eliminate the loss of the maximum allowable amplitude of the machine voltage vector, so that the operating range of the drive system can be maintained.

## References

[1] "Capacitors age and capacitors have an end of life," Emerson Network Power Co., Columbus, OH, 2008. [Online]. Available: http://www.emersonnetworkpower.com/documentation/en-us/brands/liebert/documents/white%20papers/sl-24630.pdf

[2] M. Salcone and J. Bond, "Selecting film bus link capacitors for high performance inverter applications," in *Proc. IEEE Int. Elect. Mach. Drives Conf.*, pp.1692–1699, May 2009.

[3] R. Maheshwari, S. Munk-Nielsen, and K. Lu, "An active damping technique for small dc-link capacitor based drive system," *IEEE Trans. on Ind. Inform.*, vol. 9, no. 2, pp. 848-858, May 2013.

[4] L. Mathe, H. R. Anderson, R. Lazar, and M. Ciobotaru, "DC-link compensation method for slim dc-link drives fed by soft grid," in *Proc. IEEE-ISIE*, 2010, pp. 1236–1241.

[5] M. Hinkkanen, L. Harnefors, and J. Luomi, "Control of induction motor drives equipped with small dc-link capacitance," in *Proc. EPE*, pp. 1–10, 2007.

[6] S. D. Sudhoff, K. A. Corzine, S. F. Glover, H. J. Hegner, and H. N. Robey, "DC link stabilized field oriented control of electric propulsion systems," *IEEE Trans. Energy Convers.*, vol. 13, no. 1, pp. 27–33, Mar. 1998.

[7] H. Mosskull, J. Galic, and B. Wahlberg, "Stabilization of induction motor drives with poorly damped input filters," *IEEE Trans. Ind. Electron.*, vol. 54, no. 5, pp. 2724–2734, Oct. 2007.

[8] P. Magne, D. Marx, B. Nahid-Mobarakeh, and S. Pierfederici, "Large-signal stabilization of a dc-link supplying a constant power load using a virtual capacitor: Impact on the domain of attraction," *IEEE Trans. Ind. Appl.*, vol. 48, no. 3, pp. 878–887, May/Jun. 2012.

[9] K. Pietilainen, L. Harnefors, A. Petersson, and H.-P. Nee, "DC-link stabilization and voltage sag ride-through of inverter drives," *IEEE Trans. Ind. Electron.*, vol. 53, no. 4, pp. 1261–1268, Aug. 2006.

[10] P. Liutanakul, A.-B. Awan, S. Pierfederici, B. Nahid-Mobarakeh, and F. Meibody-Tabar, "Linear stabilization of a dc bus supplying a constant power load: A general design approach," *IEEE Trans. Power Electron.*, vol. 25, no. 2, pp.475–488, Feb. 2010.

[11] Y. A.-R. I. Mohamed, A. A. A. Radwan, and T. K. Lee, "Decoupled reference-voltage-based active dc-link stabilization for PMSM drives with tight-speed regulation," *IEEE Trans. Ind. Electron.*, vol. 59, no. 12, pp.4523–4536, Dec. 2012.

[12] W.-J. Lee and S.-K. Sul, "DC-link voltage stabilization for reduced dc-link capacitor inverter," *IEEE Trans. Ind. Appl.*, vol. 50, no. 1, pp. 404–414, Jan. 2014.

[13] L. Mathe, L. Torok, D. Wang, and D. Sera, "Resonance reduction for AC drives with small capacitance in the DC link," *IEEE Trans. Ind. Appl.*, vol. 53, no. 4, pp. 3814–3820, Mar. 2017.

[14] M. Cespedes, T. Beechner, L. Xing, and J. Sun, "Stabilization of constant-power loads by passive impedance damping," in *Proc. APEC*, pp. 2174–2180, 2010.

[15] T. Nussbaumer, M. L. Heldwein, G. Guanghai, S. D. Round, and J. W. Kolar, "Comparison of prediction techniques to compensate time delays caused by digital control of a three-phase buck-type PWM rectifier system," *IEEE Trans. Ind. Electron.*, vol. 55, no. 2, pp. 791–799, Feb. 2008.

[16] D. Wang, K. Lu, P. O. Rasmussen, L. Mathe, and Y. Feng, "Analysis of voltage modulation based active damping techniques for small dc-link drive system," in *Proc. ECCE*, Montreal, Canada, Sep. 2015, pp. 2927–2934.

[17] L. Mathe, Y. Feng, and D. Wang, "Linear modeling of the three-phase diode front-ends with reduced capacitance considering the continuous conduction mode," in *Proc. IECON*, 2016.

[18] P. C. Krause, O. Wasynczuk, and S. D. Sudhoff, "Semicontrolled bridge converters," in *Analysis of Electric Machinery and Drive System*, 2nd ed., New York: Wiley-IEEE Press, 2002, pp. 395–425.

[19] R. Teodorescu, F. Blaabjerg, M. Liserre, and P. C. Loh, "Proportional-resonant controllers and filters for grid-connected voltage-source con-verters," *Proc. Inst. Electr. Eng.—Electr. Power Appl.*, vol. 153, no. 5, pp.750–762, Sep. 2006.